# Chapter 6
# Turbulent Thermal Convection and Emergence of Isolated Large Single Vortices in Soap Bubbles

**Hamid Kellay**

**Abstract** Experiments using a novel thermal convection cell consisting of half a soap bubble heated at the equator to study turbulent thermal convection and the movement of isolated vortices are reviewed. The soap bubble, subject to stratification, develops thermal convection at its equator. A particular feature of this cell is the emergence of isolated vortices. These vortices resemble hurricanes or cyclones and similarities between these structures and their natural counterparts are found. This is brought forth through a study of the mean square displacement of these objects showing signs of superdiffusion. In addition to these features, the study of the statistical properties of the turbulence engendered in these soap bubbles shows a clear indication for the existence of the so-called Bolgiano–Obukhov scaling both for the temperature and the velocity fluctuations. A remarkable transition is uncovered: the temperature and the velocity structure functions show intermittency for small temperature gradients; this intermittency then disappears for large gradients.

## 6.1 Introduction

Turbulent thermal convection is ubiquitous in several natural settings such as the atmosphere or the inner core of planets and has attracted and continues to attract considerable attention from experimentalists and theorists [1, 2]. Experiments have demonstrated several robust features of this phenomenon such as the importance of thermal plumes and the onset of a large-scale circulation [3]. Several experiments use three-dimensional geometries, but recent experiments have demonstrated similar features in two dimensions [4–6]. These experiments use vertical, stably

H. Kellay (✉)
Université Bordeaux1, LOMA UMR 5798 du CNRS,
351 cours de la Libération, 33405 Talence, France
e-mail: hamid.kellay@u-bordeaux1.fr

X. Leoncini and M. Leonetti (eds.), *From Hamiltonian Chaos to Complex Systems: A Nonlinear Physics Approach*, Nonlinear Systems and Complexity 5,
DOI 10.1007/978-1-4614-6962-9_6, 

stratified, soap films or soap bubbles [7, 8] as two-dimensional fluids. The flow occurs in the plane of the film and the velocity in the third dimension is strongly inhibited due to viscous dissipation. Soap films have now become good model systems to study two-dimensional hydrodynamics and turbulence [9] and these recent experiments extend their use to turbulent thermal convection. Interest in two-dimensional turbulence stems from the fact that atmospheric turbulence at large scales displays two-dimensional features due to the small thickness of the atmosphere [10]. According to some authors, this two dimensionality may have strong repercussions: The great red spot of Jupiter has been brought forth as a sign of the two-dimensional nature of atmospheric turbulence for example [11].

Besides its importance for the geophysical context, other fundamental issues arise. As for three-dimensional hydrodynamic turbulence [12–14], the statistical properties of temperature and velocity fluctuations in turbulent thermal convection, a state which can be reached for a high enough temperature difference between the bottom and the top of the container, can also be described by scaling laws [15,16]. While several experiments have been carried out to measure these statistical properties, a number of issues regarding the scaling properties remain unresolved [17]. In the two-dimensional version, which has been put forth recently using either vertical soap films or soap bubbles [5–7], a detailed examination of the statistical properties of the velocity fluctuations, the temperature fluctuations, and the density variations [5–8] showed that they indeed display scaling laws predicted by Bolgiano and Obukhov for stratified turbulence in the 1950s [15–17]. Such scaling laws have so far been elusive in three-dimensional experiments for reasons still debated today [17, 18].

This paper reviews the two-dimensional experiments carried out in a soap bubble and focuses both on the emergence of isolated vortices and on the statistical properties of the turbulent thermal convection produced. The paper is organized as follows: first we bring forth the emergence of these large-scale vortices and outline their specific properties, then we describe the main features of thermal convection and its statistical properties in this novel setup.

## 6.2 Isolated Vortices

A specific feature of recent experiments on soap bubbles subjected to thermal convection is the emergence and persistence of large isolated single vortices. The soap bubble (actually a half bubble is used) is heated at the equator giving rise to thermal convection. A prominent feature of this setup is the emergence of long-lived isolated vortices reminiscent of natural ones such as the red spot or hurricanes and cyclones. As we will see below, these vortices wander around the bubble randomly. The mean square displacement of these vortices varies as a power law in time. This scaling is different from the one expected for diffusive behavior and shows signs of superdiffusion. Surprisingly, analysis of the trajectories of natural hurricanes in the earth's atmosphere gives rise to a similar scaling law for their mean square

displacement versus time. Thus, the properties of these isolated vortices in this novel experimental system mimic some features of the position fluctuations of natural hurricanes. This suggests that a small experimental setup such as the one used here may allow a careful study of such large-scale phenomena of importance for atmospheric science and for meteorology. A major difference between this two-dimensional setup and previously used cells to study thermal convection is the absence of lateral walls. We believe that this absence of walls is at the origin of the emergence of long-lived isolated vortices as opposed to a large-scale circulation in cells with lateral walls.

The setup consists of a hollow brass ring with an inlet and outlet for water circulation to thermostat the full apparatus at the desired temperature. This brass ring has a circular slot which can be filled with soap water. The middle part of the ring was covered with a Teflon disk. The half bubble was blown with a straw using the soap solution in the circular slot. The ring could be kept at the desired temperature to a precision of $\pm 0.1\,^{\circ}\mathrm{C}$ using the water circulation thermostat. The temperature of the solution (the soap solution is water at different concentrations $c$ of detergent ranging from 0.2 % to 5 %) in contact with the ring and the temperature at the top of the bubble were measured using a needlelike thermistor. The temperature difference between the bottom and the top parts of the half bubble will be denoted $\Delta T$ which is our control parameter. The room was kept at a constant temperature of $17\,^{\circ}\mathrm{C}$. The difference in temperature $\Delta T$ can be changed in the range 5–45 °C. The ring has two concentric slots so we could vary the diameter of the half bubble which could be fixed to either 8 or 10 cm. Typical half bubbles with strong convective patterns are shown in Fig. 6.1. The patterns are filmed using a 3CCD camera.

Figure 6.1 shows typical half bubbles heated at the equator at different temperatures and illuminated with white light. Interference colors mark the surface of the bubble indicating variations in the thickness of the soap film. When no temperature gradient or a small gradient is present the thickness of the bubble decreases as the height increases giving rise to the horizontal bands seen in the photograph. The two-dimensional density of the soap film being $\rho h$, where $\rho$ is the density of soap water and $h$ its thickness, the film is stably stratified with dense fluid at the bottom and lighter fluid at the top. When a sufficient temperature gradient is applied, the region near the equator is host to rising plumes just like in conventional thermal convection. This convection zone extends all around the equator and grows in height as the gradient increases as shown in Fig. 6.1. The upper part of the bubble is more quiescent than the zone near the equator. No particular difference appears at this stage with conventional thermal convection. A major difference is the absence of a large-scale circulation and the emergence and persistence of single isolated vortices in the upper part of the half bubble as displayed in Fig. 6.1d. Their presence is more frequent as the temperature difference increases.

These isolated vortices emerge randomly on the surface of the bubble, grow in size rapidly as illustrated in Fig. 6.2, and persist for relatively long times almost equivalent to the lifetime of the half bubble itself which could last several minutes. The occurrence of these vortices becomes more probable for higher $\Delta T$ while they are almost absent for small $\Delta T$. At first sight, these isolated vortices move around

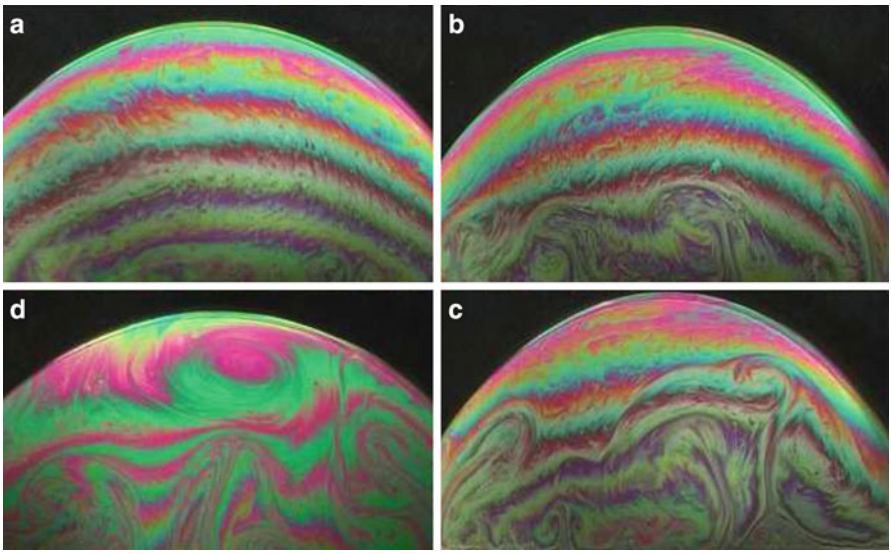


**Fig. 6.1** Images of bubbles at different temperature gradients. $\Delta T$ increases from (**a**) to (**c**) with $\Delta T = 9, 17$, and 31 °C, respectively. The convection zone grows in extent as $\Delta T$ increases. Plumes can be seen in this zone. (**d**) A bubble with a convection zone and an isolated vortex near the top for $\Delta T = 45$ °C

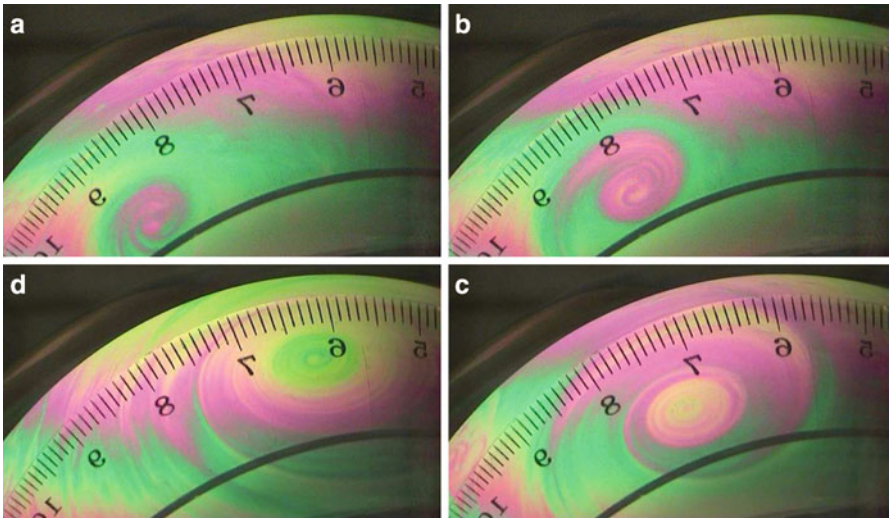


**Fig. 6.2** Birth and growth of a single vortex. The time between successive images is 0.16 s, 0.44 s, and 0.76 s. The image of a transparent ruler (in cm) was projected on the bubble

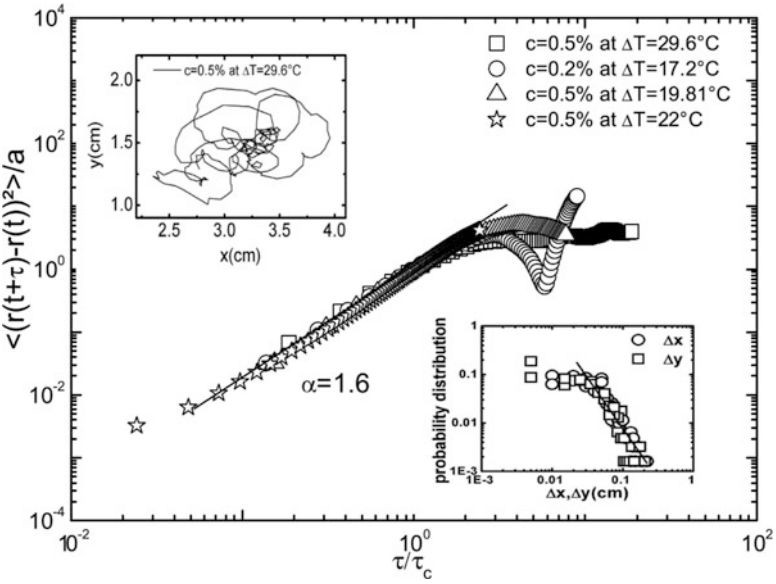


**Fig. 6.3** Mean square displacement of the isolated vortices for different $\Delta T$. *Upper inset*: a track of an isolated vortex. *Lower inset*: the pdf of the increment $\Delta$x and $\Delta$y for a fixed time interval $\Delta$t

the bubble randomly. A typical trajectory is shown in Fig. 6.3. These vortices move around the bubble with velocities near 1 cm/s. We analyze these trajectories by calculating the mean square displacement $< r^2(\tau) >=< (r(t+\tau) - r(t))^2 >$ for different time increments $\tau$. This analysis shows that $< r^2(\tau) > \sim \tau^\alpha$ with $\alpha \sim 1.6$. This scaling law is to be contrasted with Brownian motion for which the scaling exponent is 1. Figure 6.3 shows this result for different temperature differences $\Delta T$. Here we plot $\frac{<r^2(\tau)>}{<r^2(\tau_c)>}$ versus $\frac{\tau}{\tau c}$ . The characteristic time $\tau_c$ is the correlation time obtained from the correlation function $< r(t+\tau)r(t) >$. The rescaling by $\tau_c$ and the corresponding mean squared displacement $< r^2(\tau_c) >$ collapses all of the data for different temperature differences $\Delta T$. The scaling law observed is valid for more than a decade in timescales below $\tau_c$. Above $\tau_c$ the mean square displacement seems to flatten with no systematic dependence. Despite the complexity of the problem, a single scaling law summarizes all of the data and strongly suggests that these vortices are superdiffusive, a behavior observed here for the first time as far as we know. Superdiffusion arises in the so-called Lévy flights [19, 20] for which the spatial steps for a fixed time increment are distributed according to a power law $\text{pdf}(\delta r) \sim r^{-\beta}$. The exponent of this power law is directly related to the exponent $\alpha$ by the relation $\beta = 1 + 2/\alpha$. A pdf of the displacements $\Delta x$ and $\Delta y$ in the horizontal and vertical directions is shown in the inset to Fig. 6.3. A small power law range can be observed here with an exponent $\beta = 2.2$ in good agreement with that obtained

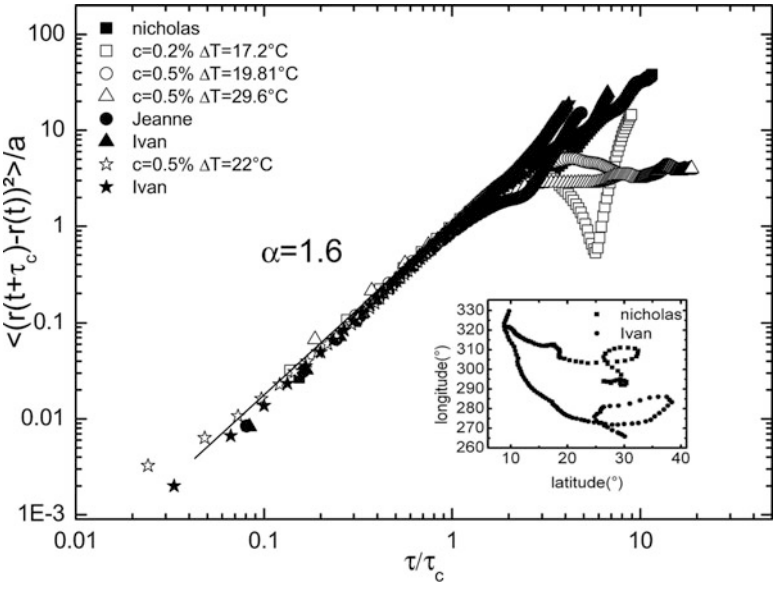


**Fig. 6.4** Mean squared displacement for natural hurricanes plotted along with some of the data from the isolated vortices in this experiment. *Lower inset*: two hurricane tracks

from the mean square displacement as indicated by the solid line. This indicates that the movement of the vortices can be recast into the random walks known as Lévy flights.

Isolated vortices occur in natural settings as well. Because of the similarities between our isolated vortices and hurricanes or cyclones we have analyzed the trajectories of certain natural hurricanes along similar lines. It should be signalled here that natural hurricanes seem to travel along relatively well-defined mean trajectories for which the Coriolis force and the beta-effect play a central role. However, they do show fluctuations around this mean trajectory. An analysis of the mean square displacement of different hurricanes including Nicholas (2003), Jeanne (2004), and Ivan (2004) shows a very similar behavior as our isolated vortices. The hurricane trajectories were obtained from the National Hurricane Center web site and consist of either satellite observations or of radar data. Their trajectories are sampled every 6 h for satellite data and every 15 min for radar data. The analysis of these trajectories is summarized in Fig. 6.4 where the trajectories are displayed in the inset. Here, the data of Fig. 6.3 are replotted so as to illustrate the similarity. This plot shows that the hurricanes and our isolated vortices display very similar features especially the power law scaling at times smaller than $\tau_c$. The scaling exponent turns out to be very close to the value extracted from our vortices, namely, $\alpha = 1.6$.

Superdiffusive behavior can be traced to a nontrivial interaction between the moving object and the medium. An example of entities that interact with the medium itself has been illustrated through a study of the superdiffusion of passive beads in

a bath of self-propelling bacteria [21]. Another example concerns the movement of passive beads in a laminar rotating flow where vortices may trap and release the particles giving rise to superdiffusion [22]. The isolated vortices here are kicked by the turbulent agitation of the surrounding flow. These vortices, being part of the flow, must have an important reaction on the medium itself. In addition, the movement of vortices is sensitive to the sign of vorticity gradients [23] which in a turbulent medium may show a complicated spatial and temporal distribution and a nontrivial interaction with the moving vortex giving rise to a complex trajectory and dynamics.

## 6.3 Statistical Properties of the Temperature and Velocity Fields

As stated above, the turbulent convection produced in such a cell can be characterized with respect to the velocity and temperature fluctuations. And a question that needs to be answered is about the relevance of known scaling laws to this situation. The two-dimensional nature of the system allows for tests that are difficult to carry out in three dimensions. We therefore explored the temperature field in this unusual thermal convection cell: half a soap bubble heated from below (see Fig. 6.1) [7]. As mentioned above, this geometry has the advantage of avoiding the presence of side walls and therefore the presence of the large-scale circulation often observed when lateral walls are present. By focusing on the structure functions of the temperature field a transition from an intermittent to a non-intermittent behavior has been observed. The results show that the scaling of these functions switches regimes from the so-called Obukhov–Corrsin-like scaling [13, 14] with intermittency at low temperatures to Bolgiano–Obukhov-like scaling without intermittency at higher temperatures. Our results are unique and surprising since previous numerical work indicated the presence of strong intermittency for the temperature field [24, 25]. Intermittency in fluid turbulence is an important problem in hydrodynamics and our experiments bring to light how a simple system evolves from an intermittent to a non-intermittent state.

The setup is in a room kept at a constant temperature of 17 °C with a humidity rate of nearly 75 % near the bubble. The temperature gradient between the bottom and the top of the half bubble $\Delta T$ could be varied up to 55 °C. The temperature measurements used a calibrated 14 bit infrared camera (resolution $256 \times 360$) working in the spectral range 3.6–5 $\mu$m with a sensitivity of 20 mK and an adjustable exposure time set between 0.5 and 1 ms. Images of the same region (between 100 and 500 images at a rate of 50 or 100 frames/second) were recorded and a homemade program was used to calculate temperature differences across different scales $r$. Averaging over the area of interest and over several images allowed us to improve the statistics (between 1 and 2.5 million points were used) and calculate the high-order moments of these differences. The temperature field was recorded for periods of up to 10 s which is greater than the temperature correlation time (of order 0.1 s).

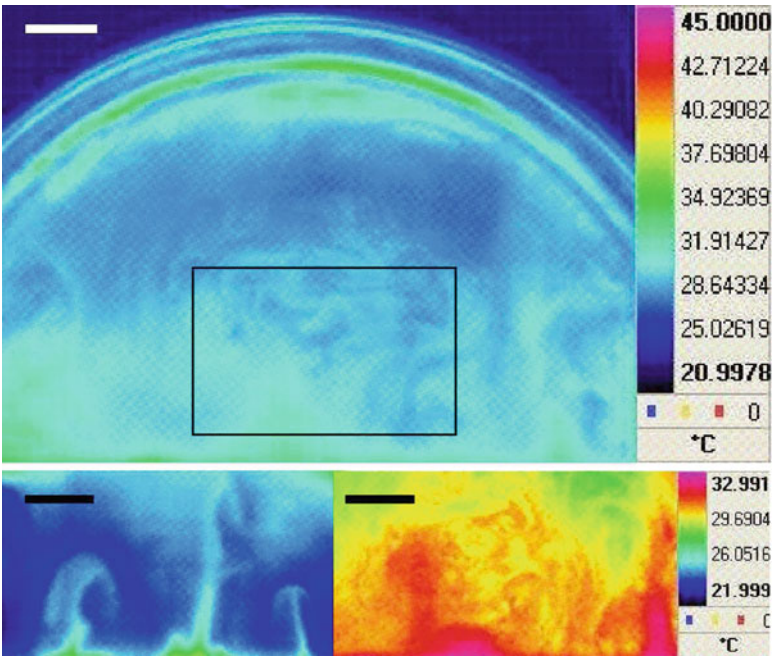


**Fig. 6.5** Infrared images of the bubble (*top* $\Delta T = 50\,^{\circ}\mathrm{C}$) and a region near the *bottom*: $\Delta T = 21\,^{\circ}\mathrm{C}$ (*bottom left*) and $50\,^{\circ}\mathrm{C}$ (*bottom right*). The region delimited by a *rectangle* in the upper image indicates the area covered by the temperature and velocity measurements. The *brass ring* is located a few millimeters from the bottom of the images

The error in $r$, introduced by the curved geometry of the bubble, turned out to be less than a few percent over a 1 cm region. The effect of evaporation was estimated to be small and the lifetime of the bubble, which should decrease with increased evaporation, actually increases by a factor of about 4 when a temperature gradient is imposed indicating that convection is more important than both evaporation and draining by gravity.

Figure 6.5 shows a full view of the bubble as well as images obtained with the infrared camera in a region near the bottom of the half bubble where the thermal convection is strongest. One can easily identify thermal plumes rising from the bottom of the cell which are clearly visible for the low temperature gradient. The thermal convection becomes more intense as the temperature gradient increases and well-defined thermal plumes are difficult to discern. From such spatial images we extract the temperature difference $\delta T(r_x) = T(x + r_x) - T(x)$ and $\delta T(r_y) = T(y + r_y) - T(y)$ and calculate the $n$th moments as $< |\delta T(r_x)|^n >$ and $< \left|\delta T(r_y)\right|^n >$. Here $x$ and $y$ refer to the horizontal and vertical coordinates and the brackets refer to an average over space and time. The temperature structure functions are important quantities in the study of turbulence and different scaling relations have been proposed for their variation versus the scale $r$. In 3D turbulent flows, where

Kolmogorov-like scaling is believed to prevail for the low-order moments, Obukhov and Corrsin [13, 14] generalized the scaling arguments of Kolmogorov to a scalar field like the temperature and used both the energy dissipation rate $\varepsilon$ and the scalar dissipation rate $\varepsilon_\theta$ to predict that the second-order structure functions should scale as $\varepsilon_\theta \varepsilon^{-1/3} r^{2/3}$. Similar scaling arguments can be used, as suggested by Bolgiano and Obukhov [15–17] for stably stratified turbulence, to the case of Rayleigh-Benard convection for which the fluid thermal expansion rate $\beta$, the gravity constant $g$, and the dissipation rate $\varepsilon_\theta$ fix the scaling relation of the second-order structure function of the temperature as $\varepsilon_\theta^{4/5} (\beta g)^{-2/5} r^{2/5}$ [17]. The $n$th order moments are expected to vary as a power law of the separation distance $r$ with an exponent $\zeta_n^T$ of $n/5$ in the Bolgiano–Obukhov regime and $n/3$ for the Obukhov–Corrsin regime. To compare the experimental conditions here to their classical counterparts, we estimated the Rayleigh number ($Ra = \beta \Delta T g R^3 / \nu \kappa$ where $\nu$ and $\kappa$ are the kinematic viscosity and the thermal diffusivity of water) to be between $7 \times 10^7$ and $2 \times 10^8$ while the Reynolds number ($Re = V_{\text{mean}} R / \nu$ where $V_{\text{mean}}$ is the characteristic horizontal velocity) is estimated to be about 3,000.

The temperature structure functions are displayed in Fig. 6.6a, b for two different $\Delta T$: 21 °C and 50 °C. For the low $\Delta T$, Fig. 6.6a, the temperature structure functions are roughly isotropic as the values of the differences for the two orthogonal spatial increments $r_x$ and $r_y$ are similar. These functions display power law scaling for spatial scales between roughly 1 and 10 mm as the compensated moments show. The scaling exponents vary in a nontrivial manner versus the order $n$ of the moment. This exponent is in agreement with predictions of Obukhov and Corrsin [13, 14] for low n in Kolmogorov-like turbulence [12]. However, for higher moments, the exponents deviate from this prediction. The growth is nonlinear versus n which is the hallmark of intermittency. The relation between the higher-order moments and the low-order ones is nontrivial indicating that the functional shape of the probability distribution functions of the increments varies with $r_x$ or $r_y$. This behavior is similar to that observed in three-dimensional experiments where Bolgiano-like scaling has not been observed so far; rather Obukhov–Corrsin scaling with deviations, just like passive scalar fields in three-dimensional hydrodynamic turbulence, is observed [17, 18, 26].

The high $\Delta T$ results are shown in Fig. 6.6b. While the structure functions show isotropy and power law scaling versus $r$, the variation of the exponents versus n turns out to be different from the previous results. Bolgiano–Obukhov-like scaling is observed in the range 1–10 mm as shown in Fig. 6.6b which displays the compensated moments as well as the scaling exponents extracted from such an analysis. Estimates of the Bolgiano length scale (above which such a scaling is believed to prevail) give $L_B \sim 1$ mm which is in good agreement with the range observed here and in previous experiments using vertical films [5, 6]. The surprising aspect is that a linear variation of the exponents versus n is observed. This linear variation indicates that intermittency is absent. This behavior has been observed for an imposed $\Delta T$ higher than about 35 °C.

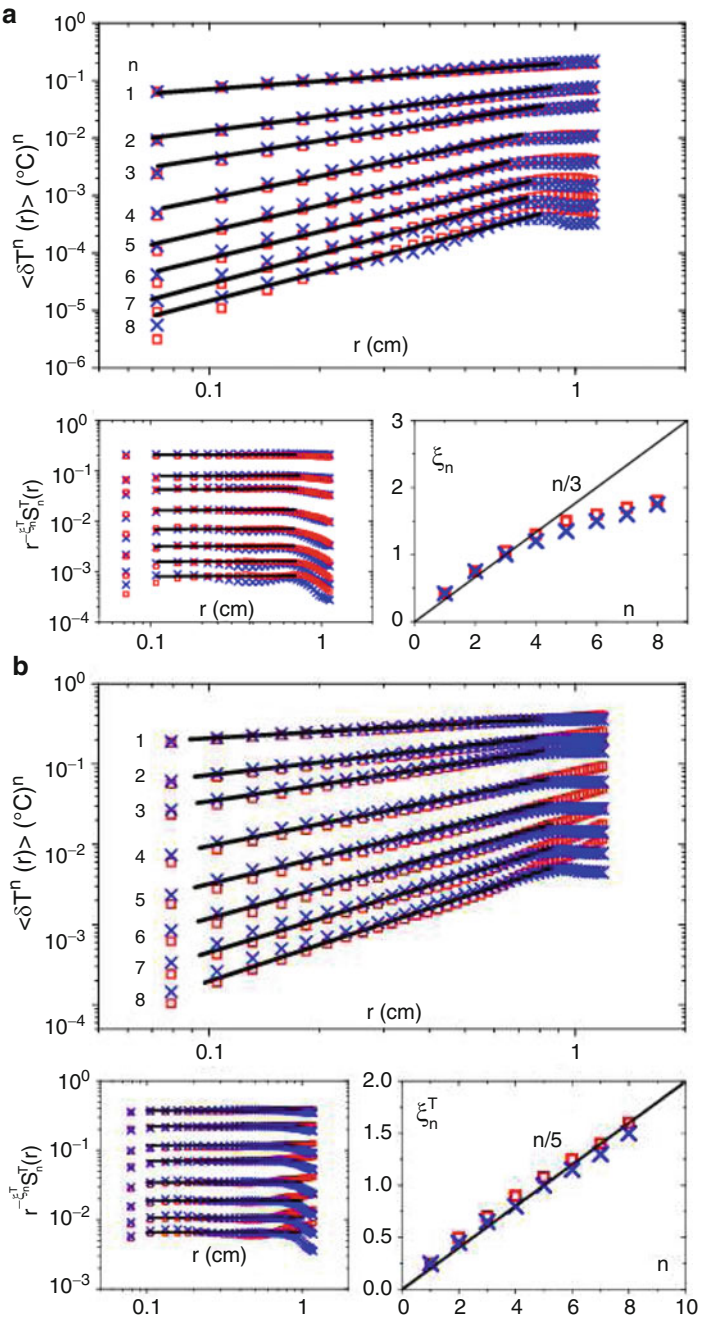


**Fig. 6.6** Temperature structure functions for $\Delta T = 21\,^{\circ}\mathrm{C}$ (**a**) $\Delta T = 50\,^{\circ}\mathrm{C}$ (**b**). The *horizontal* (*squares*) and *vertical* (*crosses*) components are plotted up to order 8. The data is shifted by a multiplicative factor (x2 for n = 3 up to x64 for n = 8). Insets: compensated moments and scaling exponents

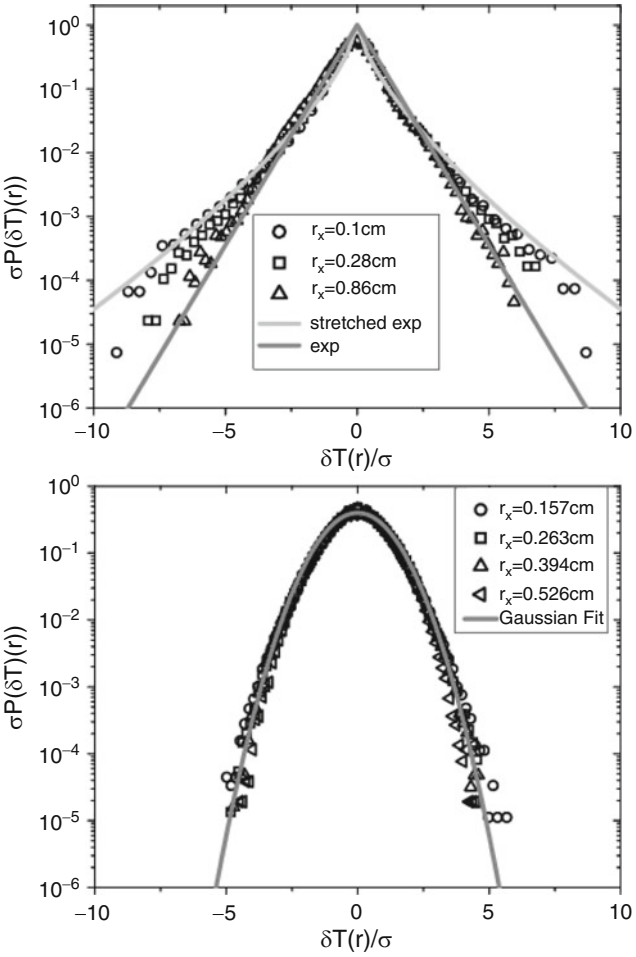


**Fig. 6.7** Pdfs of temperature increments for $\Delta T = 21\,^{\circ}\mathrm{C}$ (*upper set*) $\Delta T = 50\,^{\circ}\mathrm{C}$ (*lower set*). The axes were rescaled by the standard deviation $\sigma$ of the increments. *Solid lines*: fits using a stretched exponential function and an exponential function. A Gaussian function is used in the lower set of pdfs

Additional insight into this transition comes from an examination of the probability density functions (pdfs) of the temperature increments in the range of scales for which power laws are observed. These results are shown in Fig. 6.7. The horizontal axis has been rescaled by the standard deviation $\sigma(=\sqrt{<|\delta T(r)|^2>})$ of the temperature increment at the scale $r$ while the vertical axis has been normalized in such a way that the integral of the function is unity. Note that for the small gradient, the pdfs start out as a stretched exponential with an exponent near 0.7 at the small-scale end of the scaling range (1 mm) and end up as an exponential

for the large-scale end (9 mm). The pdfs evolve gradually as the scale increases from 1 to 10 mm, indicating a change of the functional shape of the pdf across the scales. For the high $\Delta T$, the pdfs remain roughly Gaussian as the scale changes from 0.9 up to 8 mm. The normalization of the pdfs by $\sigma$ collapses all the pdfs together indicating that they depend solely on the width of the distribution. An examination of the flatness of these pdfs shows that for the low $\Delta T$, the flatness decreases from roughly 10 to 5 as the scale increases from 1 to 10 mm. On the other hand, the flatness for the high $\Delta T$ case remains roughly constant near a value of 2.8 which is not far from the flatness of a Gaussian distribution. These features are at the origin of the dependence of the scaling exponents versus n. In short, intermittency of the scaling exponents is associated with the gradual change of the functional shape of the probability density of temperature increments. On the other hand, the absence of intermittency is related to the Gaussian pdfs of the increments all through the scaling range.

To complement these observations, we measured the velocity fluctuations at a single point and constructed the one-dimensional velocity spectra as well as the horizontal velocity structure functions of order n as $< |\delta V(\delta t)|^n >$ where $\delta t$ is a temporal increment. These measurements use a Laser Doppler Velocimeter and a soap solution seeded with 1 $\mu$m-sized polystyrene spheres. We record between $5 \times 10^5$ and $5 \times 10^6$ points over a total period of time of nearly 100 s which is greater than the velocity correlation time (0.2 s). The choice of the horizontal component of the velocity $V$ is justified by the presence over sufficiently long periods of time of a mean flow in this direction, at the location of the measurements, allowing the use of the Taylor frozen turbulence hypothesis to convert $\delta t$ to a scale $r$ as $r = V_{\text{mean}} \delta t$. This hypothesis is not tested here however. The velocity structure functions are expected to vary as power laws of $r$ with an exponent $\zeta_n^V = 3n/5$ following similar arguments as for the temperature in the Bolgiano–Obukhov regime.

The properties of the convective zone share some similarities with those observed in experiments of convection in vertical soap films. A common feature is the scaling of the velocity field. The results of Zhang and Wu [6] show that in the turbulent regime obtained for high $\Delta T$, the second-order structure function of the velocity differences scales as $<\delta v^2(r)> = < (v(r) - v(0))^2 > \sim r$. This scaling is consistent with Bolgiano's prediction [15] for the energy density spectrum which reads: $E(k) \sim k^{-11/5}$. Our results for the velocity spectra are displayed in Fig. 6.8. The horizontal axis is frequency because the one-point measurements are time series of the velocity. The frequency axis can be converted to a wave number in the direction of the mean flow using Taylor's frozen turbulence assumption. The mean velocity here is horizontal so the wave number is in the horizontal direction and is given by $k_x = 2\pi f / V_{\text{mean}}$. A histogram of the horizontal velocity fluctuations is shown in the inset to Fig. 6.8 showing a well-defined nonzero velocity. The scaling obtained from our data gives an exponent of $-2.2$ which is consistent with the findings of Zhang and Wu [6] and is in agreement with the Bolgiano scaling expected for the buoyancy subrange of turbulence in stably stratified fluids [15].

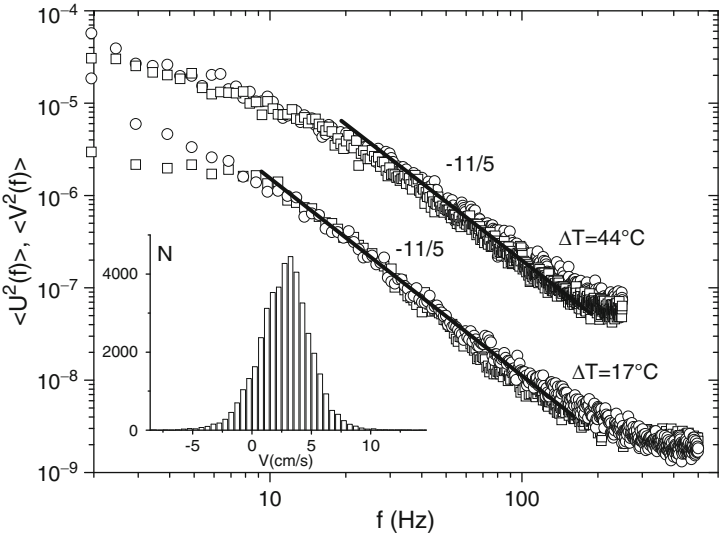


**Fig. 6.8** Velocity spectra in the convection zone. *Circles* are for the vertical velocity while *squares* are for the horizontal velocity. The *solid line* is the Bolgiano prediction. Inset: a histogram of the horizontal velocity fluctuations for $\Delta T = 44\,^{\circ}\mathrm{C}$

The structure functions of the velocity differences are displayed in Fig. 6.9a, b for the low and high $\Delta T$, respectively. Power laws are obtained for the different moments examined. The variation of the exponents, obtained from an analysis of the compensated moments, is nonlinear for the low $\Delta T$ case and linear for the higher one. The expected $3n/5$ variation is shown as a solid line. The scaling range in $r$, determined using the Taylor hypothesis, turns out to be similar to that obtained from the temperature structure functions. The variation of the exponents for the low $\Delta T$ case (as well as the flatness of the distributions which decreases from roughly 10 to nearly 3) is similar to that obtained by Zhang and Wu [6]. The agreement between our results and the spatial measurements of Zhang and Wu seems to validate our use of the Taylor hypothesis for this case. The low temperature gradient statistics therefore show that intermittency is observed for both the velocity and the temperature. For the high $\Delta T$, the scaling exponents vary linearly with $n$ and follow the $3n/5$ law in good agreement with the predictions of Bolgiano and Obukhov for the same range of scales $r$ as the temperature. The flatness of the distributions in this case remains roughly constant near a value of 5. These results are therefore consistent with the temperature measurements and indicate an absence of intermittency for the velocity as well. The Taylor hypothesis in this case has not been tested however and the results of Zhang and Wu did not show an absence of intermittency in their rectangular cells for similar temperature gradients. Our results, even though consistent with the temperature measurements, would need additional confirmation. We noted by examining the pdfs of velocity differences that their

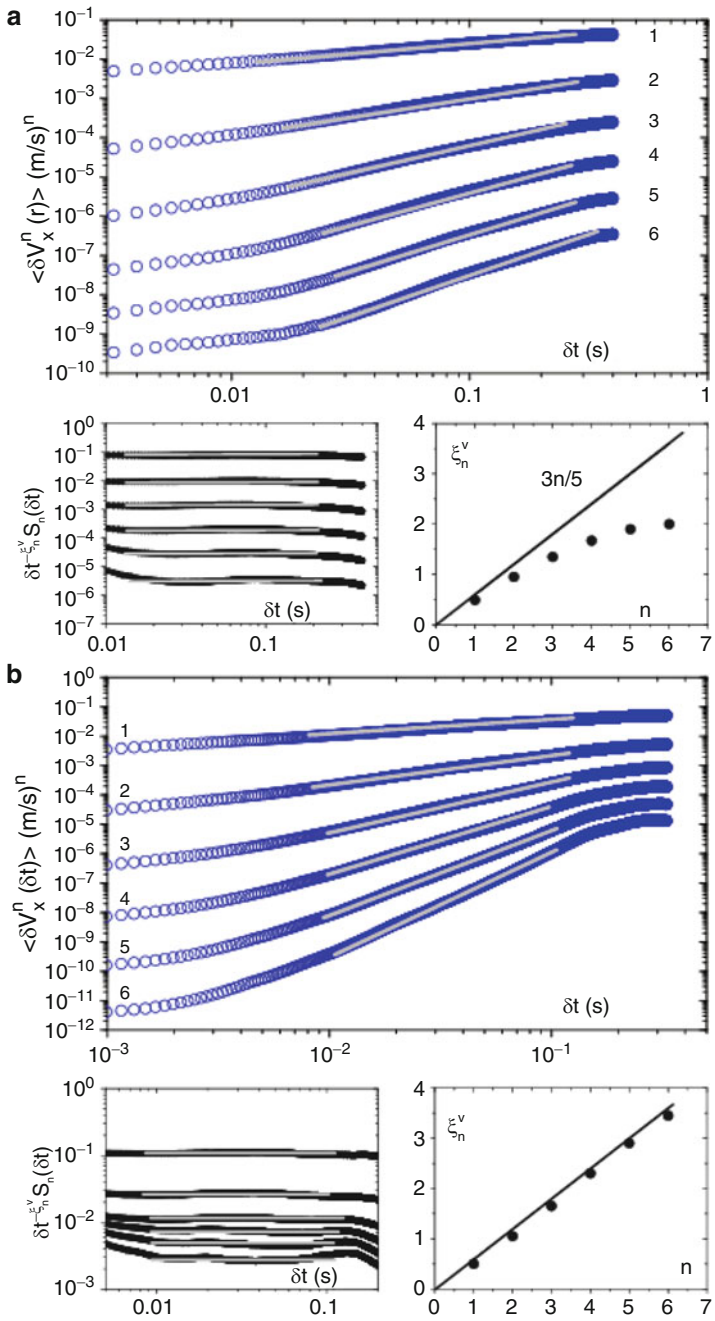


**Fig. 6.9** $(< |\delta V(\delta t)|^n >$ for $\Delta T = 21\,^\circ$C (**a**) $\Delta T = 50\,^\circ$C (**b**). The mean horizontal velocity is 5 cm/s in (a) and 8 cm/s in (b). Insets: compensated moments and scaling exponents

evolution with $\Delta T$ is less convincing than that of the temperature: while a better collapse can be achieved for the high $\Delta T$ case, the pdfs are not Gaussian and show roughly exponential tails.

## 6.4 Conclusion

In conclusion, our novel quasi two-dimensional convection cell allows for a detailed study of the statistical properties of temperature fluctuations in turbulent thermal convection. These properties show that a transition from an intermittent state to a non-intermittent one occurs as the temperature gradient increases. Bolgiano–Obukhov-like scaling with no intermittency is recovered for the high-gradient case. Our results raise fundamental questions about the role of lateral walls and the ensuing large-scale circulation often observed in traditional convection cells as well as the role of thermal plumes in setting the properties of temperature fluctuations in turbulent thermal convection.

In addition, our experiments show that the curved nature of the bubble used allows for isolated vortices to emerge. The absence of walls is the most probable reason for the emergence of such structures. These isolated vortices resemble natural hurricanes for certain aspects. In particular, when the mean squared displacement of the eye is examined superdiffusion is recovered. This superdiffusion is probably indicative of Lévy flights and calls for further theoretical work on the movement of isolated vortices in a turbulent medium which is important for turbulence in general and for atmospheric and meteorological studies in particular.

**Acknowledgements** This work was carried out with my colleagues (M. Bessafi and Y. Amarouchene) and students (F. Seychelles, F. Ingremeau, T. Meuel, G. Prado) to whom I am very grateful. This work was supported by Grant "Cyclobulle" from the ANR.

## References

1. L.P. Kadanoff, Phys. Today **54**, 34 (2001)
2. E.D. Siggia, Ann. Rev. Fluid Mech. **26**, 137 (1994)
3. G. Ahlers, Physics, **2**, 74 (2009)
4. B. Martin, X.L. Wu, Phys. Rev. Lett. **80**, 1892 (1998)
5. J. Zhang, X.L. Wu, K.Q. Xia, Phys. Rev. Lett. **94**, 174503 (2005)
6. J. Zhang, X.L. Wu, Phys. Rev. Lett. **94**, 234501 (2005)
7. F. Seychelles et al., Phys. Rev. Lett. **100**, 144501 (2008)
8. F. Seychelles, F. Ingremeau, H. Kellay, Phys. Rev. Lett. **105**, 264502 (2010)
9. H. Kellay, W.I. Goldburg, Rep. Prog. Phys. **65**, 1 (2002).
10. P. Morel, M. Larcheveque, J. Atmos. Sci. **31**, 2189 (1974)
11. P.S. Marcus, Nature **428**, 828 (2004)
12. A.N. Kolmogorov, Dokl. Akad. Nauk. SSSR **30**, 299 (1941)
13. S. Corrsin, J. Appl. Phys. **22**, 469 (1951)

14. A.M. Obukhov, Izv. Akad. Nauk SSSR Ser. Geog. Geofiz **13**, 58 (1949)
15. R. Bolgiano, J. Geophys. Research **64**, 2226 (1959)
16. A.M. Obukhov, Sov. Phys. Dokl. **4**, 61 (1959)
17. D. Lohse, K.-Q. Xia, Annu. Rev. Fluid Mech. **42**, 335 (2010)
18. C. Sun, Q. Zhou, K.-Q. Xia, Phys. Rev. Lett. **97**, 144504 (2006)
19. M.F. Shlesinger, G.M. Zaslavsky, U. Frisch (eds.), Levy Flights and Related Topics in Physics. Lecture Notes in Physics (Springer, Berlin, 1995)
20. J.P. Bouchaud, A. George, Phys. Rep. **195**, 127 (1990)
21. X.L. Wu, A. Libchaber, Phys. Rev. Lett. **84**, 3017 (2000)
22. T.H. Solomon, E.R. Weeks, H.L. Swinney, Phys. Rev. Lett. **71**, 3975 (1993)
23. D.A. Schecter, D.H.E. Dubin, Phys. Rev. Lett. **83**, 2191 (1999)
24. A. Celani, A. Mazzino, M. Vergassola, Phys. Fluids **13**, 2133 (2001)
25. A. Celani et al., Phys. Rev. Lett. **88**, 054503 (2002)
26. Z. Warhaft, Annu. Rev. Fluid Mech. **32**, 203 (2000)